Engineering xxx (xxxx) xxx

Contents lists available at ScienceDirect

Engineering

journal homepage: www.elsevier.com/locate/eng

Research
Sustainable and High-Performance Structural Materials—Article

Imparting Ductility to FRP-Reinforced Concrete Beams Through Compression Zone Confinement

Shi-Shun Zhang [a,b], Xiao-Bing Hu [a], Jin-Guang Teng [c,*]

[a] School of Civil and Hydraulic Engineering, Huazhong University of Science and Technology, Wuhan 430074, China
[b] National Center of Technology Innovation for Digital Construction, Huazhong University of Science and Technology, Wuhan 430074, China
[c] Department of Civil and Environmental Engineering, The Hong Kong Polytechnic University, 999077, Hong Kong, China

ARTICLE INFO

Article history:
Received 29 January 2025
Revised 21 February 2026
Accepted 20 April 2026
Available online xxxx

Keywords:
FRP bar-reinforced concrete (FRP-RC) beam
Ductility
FRP confinement
Compression zone
Load-carrying capacity

ABSTRACT

In recent decades, fiber-reinforced polymer (FRP) bar-reinforced concrete (FRP-RC) beams have attracted considerable attention as a corrosion-free beam form. However, FRP-RC beams have limited practical applications owing to their much lower ductility compared to conventional steel bar-reinforced concrete (steel-RC) beams. To improve the ductility of FRP-RC beams, this study presents an innovative sectional form for FRP-RC beams in which the compression zone concrete is confined with FRP spirals/hoops. With such a sectional form, the ductility of the beam is derived from the ductile behavior of confined concrete in the compression zone instead of the ductile behavior of steel yielding in a conventional steel-RC beam. An experimental program consisting of eight large-scale FRP-RC beams was conducted to validate the effectiveness of this sectional form, in which the variables investigated include the pitch of the FRP spiral used to offer confinement, amount of longitudinal tension FRP bars, and FRP confinement configuration. The test results demonstrate the effectiveness of FRP confinement in improving the ductility and load-carrying capacity of FRP-RC beams; for one of the beams tested in the present study, ductility was increased by 150% with only a corresponding cost increase of around 7%. The significant effects of design parameters on the behavior of such FRP-RC beams are clearly revealed. Finally, a finite element model for such FRP-RC beams was established and verified using the test results.

1. Introduction

The application of fiber-reinforced polymer (FRP) composites in civil engineering has led to considerable research in recent decades [1–6], and this growing popularity of FRP composites is due to their high strength-to-weight ratio, corrosion resistance, and life cycle cost–effectiveness [7]. The substitution of steel reinforcements with FRP bars in reinforced concrete beams is one of the most popular applications of FRP composites and has been extensively investigated [8,9]. Studies have shown that FRP bar-reinforced concrete (FRP-RC) beams can achieve excellent corrosion resistance and load-carrying performance. However, unlike conventional steel bar-reinforced concrete (steel-RC) beams that exhibit ductile flexural behavior, FRP-RC beams normally fail in a brittle manner, exhibiting a virtually bilinear load–deflection response without a yield plateau [10]. Ductility is one of the most important factors in the design of flexural members, along with strength and stiffness [11,12]. For conventional steel-RC beams, ductility is primarily derived from the yielding of the tension steel reinforcement, which is unavailable in FRP-RC beams. Consequently, FRP-RC beams are usually designed as over-reinforced beams so that the brittle failure mode owing to the sudden tensile rupture of FRP bars [13,14] is avoided, whereas a certain level of ductility is achieved from the nonlinear compressive crushing process of concrete. However, the ductility achieved using this design approach is limited [15,16].

To improve the flexural ductility of FRP-RC beams, five different methods have been explored to enhance the ductility of the compression zone of such beams: ① embedding a compression yielding (CY) block, which can be based on steel [17,18] or fiber-reinforced concrete [19], in the compression region of the beam; ② using FRP-UHPC (ultra-high performance concrete) hybrid rebars as compression bars in the member [20,21]; ③ adopting fiber-reinforced concrete [22] or engineered cementitious composites (ECCs) [23] to cast the beam; ④ confining the entire beam section with densely arranged FRP stirrups [24]; and

* Corresponding author.
E-mail address: cejgteng@polyu.edu.hk (J.-G. Teng).

https://doi.org/10.1016/j.eng.2026.04.012

Please cite this article as: S.-S. Zhang, X.-B. Hu and J.-G. Teng, Imparting Ductility to FRP-Reinforced Concrete Beams Through Compression Zone Confinement, Engineering, https://doi.org/10.1016/j.eng.2026.04.012

⑤ confining compression-zone concrete with either a flexible hollow section formed from a continuous carbon fiber sheet [24] or an FRP tube (Option 1) [25], with carbon fiber sheet ribbons (Option 2) [26], or with FRP helical reinforcement (i.e., FRP spirals, Option 3) [27,28]. Method 1 can be very effective in improving the ductility of a simply supported beam. However, when it is implemented in real structures that are likely to be exposed to a wide range of loading with a significant degree of uncertainty (e.g., the effect of foundation settlement), it is difficult to ensure in design and construction that enough CY blocks are provided and they are all located at the critical locations. Method 2 involves a relatively complex process of hybrid rebar fabrication and installation. Method 3 offers only limited enhancement in the ductility of the beam, while concomitantly increasing the costs of the materials. Method 4 usually requires the use of a large amount of FRP, and densely arranged FRP stirrups can cause difficulties in the *in situ* casting of concrete [24]. Method 5, which imparts ductility through compression zone confinement (CZC), appears to be the most promising.

Among the three options of Method 5, Option 3 was the most attractive, as explained below. In Option 1, the use of a tube formed from a continuous carbon fiber sheet or an FRP tube to confine the compression-zone concrete can cause difficulties in the *in situ* casting of concrete, and the presence of the tube also compromises the integrity of the beam. In Option 2, controlling the shapes and positions of the soft carbon fiber sheet ribbons during concrete casting is challenging. Option 3 introduces a novel strategy for utilizing FRP spirals to confine concrete within the compression zone, thereby significantly enhancing its compressive strength and ultimate strain. Previous studies have demonstrated that FRP spiral confinement can substantially improve the mechanical properties of concrete, including its deformation capacity [29–32]. This mechanism facilitates the formation of a CY plastic hinge, significantly enhancing the ductility of the flexural members [28]. Additionally, Option 3 avoids the issues associated with Options 1 and 2: the segregation issue between the FRP tube and the rest of the beam is eliminated, and the spirals possess sufficient stiffness for shape and position retention.

The innovative sectional form of an FRP-RC beam of Option 3 was studied through limited beam testing and was found to be effective in enhancing the deformation and ductility of the beam [28]. In the present study, eight large-scale beam tests were conducted to systematically investigate the failure mechanism and flexural behavior of FRP-reinforced CZC concrete beams (hereafter FRP-CZC beams, or FRP-RC beams for short). The investigated parameters include the pitch of the FRP spiral, longitudinal tension FRP reinforcement ratio, and FRP confinement configuration (i.e., continuous circular FRP spiral, continuous rectangular FRP spiral, and discrete circular FRP hoops). Furthermore, a three-dimensional (3D) nonlinear finite element (FE) approach was established to simulate the behavior of FRP-CZC beams, and its accuracy was verified using the test results. In this study, the ductility of such FRP-CZC beams was demonstrated, the failure mechanism was clarified, and the effects of key design parameters on the flexural behavior were revealed. This study provides improved insight into the performance of FRP-CZC beams and offers a useful experimental and numerical basis for further studies.

2. Experimental program

2.1. Test specimens

The test program consisted of eight large-scale FRP-RC beams. Glass FRP (GFRP) bars were used as longitudinal and shear FRP reinforcements, and they were also used to confine the compression zone. Fig. 1 shows the dimensions and configurations of the internal FRP reinforcements of the test beams. The figure indicates that all the test beams were 200 mm wide, 300 mm high, and 3100 mm long, and the clear concrete cover was 20 mm thick. The test beams had a pure bending region of 600 mm, and two shear spans of 1000 mm each. Two GFRP bars with a diameter of 12 mm (2G12) were placed in the compression zone of each beam. To avoid shear failure of the beams, densely placed transverse GFRP stirrups with a diameter of 12 mm and a spacing of 50 mm (G12@50) were adopted in the two shear spans of the beams, whereas a spacing of 200 mm was used for the stirrups in the pure bending region of the beams. To avoid brittle failure of the beams owing to the early rupture of the longitudinal tension reinforcement, all test beams had a large amount of longitudinal tension GFRP bars, leading to longitudinal reinforcement ratios larger than the balanced reinforcement ratio of the corresponding beam without FRP confinement according to the relevant Chinese national standard [33].

Among the eight test beams, one was the control beam (CB) without FRP confinement in the compression zone. The remaining seven beams were provided with FRP confinement of different configurations, including: a continuous circular FRP spiral (pitches of 40, 50, or 67 mm), a continuous rectangular FRP spiral (50 mm pitch), or discrete circular GFRP hoops (50 mm spacing). These hoops were formed by cutting circular spirals into discrete rings with approximately a one-third circumference overlap at the ends. Furthermore, the effects of different longitudinal FRP reinforcement ratios (1.44%, 1.83%, and 2.88%) on FRP confinement were considered. The FRP reinforcement cages for some test beams are shown in Fig. 2. The specimens include CB and the FRP-RC beams designated as CS40-3G20/12, CS50-3G25, CS67-3G25, CH50-3G25, and RS50-3G25. In the specimen names, CS, RS, and CH denote circular spiral, rectangular spiral, and circular hoops, respectively, followed by the pitch/spacing of FRP spiral/hoops in millimeters; the suffix indicates the details of longitudinal GFRP bars. For example, CS40-3G20 refers to an FRP-RC beam reinforced with three 20 mm longitudinal GFRP bars and confined in the compression zone by a circular spiral at 40 mm pitch.

Table 1 summarizes the details of the longitudinal FRP reinforcement and FRP confinement for all the test beams.

2.2. Material properties

All test beams were cast with the same batch of normal-weight ready-mixed concrete provided by a local commercial concrete supplier and cured for more than 28 days. The coarse aggregate used to cast the concrete was well-graded crushed stone with a maximum nominal size of 20 mm. The concrete material properties were obtained from compression tests of standard concrete cylinders (150 mm in diameter × 300 mm in height) according to ASTM C39/C39M-18 [34]. The average compressive strength of the concrete was 50.2 MPa.

Pultruded GFRP bars with different diameters were used in the beams, as shown in Fig. 3. The longitudinal/shear GFRP bars (G12, G20, and G25 with diameters of 12, 20, and 25 mm, respectively) had a deep-ribbed surface to ensure strong bonding with concrete. The tensile properties of the GFRP bars were determined via tensile tests according to ASTM D7205/D7205M-11 [35]. To determine the tensile properties of the GFRP spirals and hoops, the corresponding GFRP straight bars with the same raw materials (continuous glass fibers and resin) were tested under tension. Table 2 summarizes the tensile properties of the GFRP bars averaged from five samples. The GFRP spirals or hoops (G9-1 in Table 2) had an inner diameter of 114 mm, while the rectangular GFRP spirals (G9-2 in Table 2) had the same inner width and height of 112 mm (i.e., square spirals), as shown in Fig. 3(b). All the FRP spirals were manufactured

Please cite this article as: S.-S. Zhang, X.-B. Hu and J.-G. Teng, Imparting Ductility to FRP-Reinforced Concrete Beams Through Compression Zone Confinement, Engineering, https://doi.org/10.1016/j.eng.2026.04.012

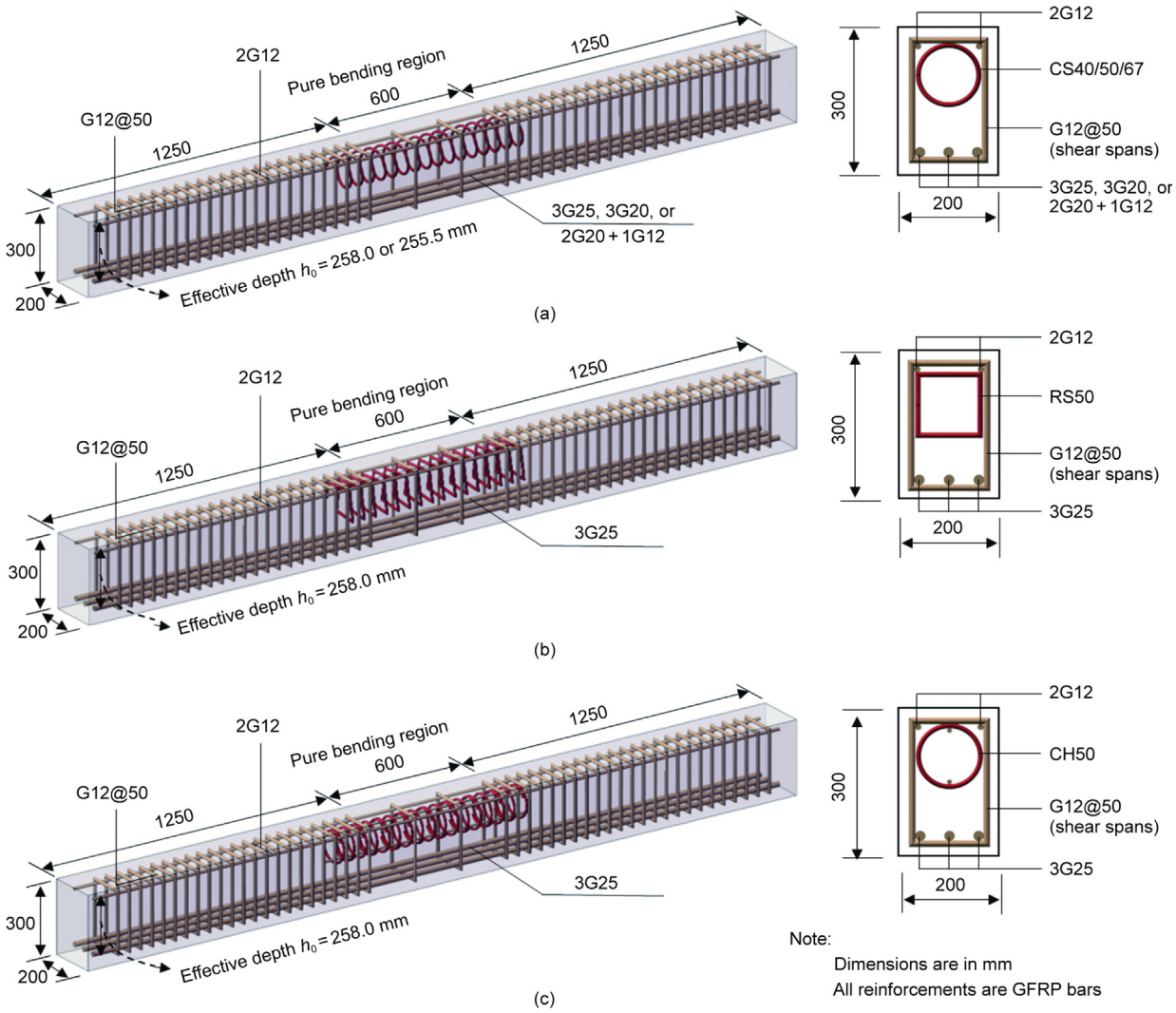

Fig. 1. Dimensions and reinforcement details of test beams. (a) Confined with a circular FRP spiral; (b) confined with a rectangular FRP spiral; (c) confined with circular FRP hoops. 3G25 and 3G20 represent three GFRP bars with a diameter of 25 mm and 20 mm, respectively; 2G20+1G12 represents two GFRP bars with a diameter of 20 and one GFRP bar with a diameter of 12 mm; CS40/50/67 denotes a continuous circular FRP spiral with a pitch of 40, 50, or 67 mm; RS50 denotes a continuous rectangular FRP spiral with a pitch of 50 mm; CH50 denotes discrete circular GFRP hoops with a spacing of 50 mm.

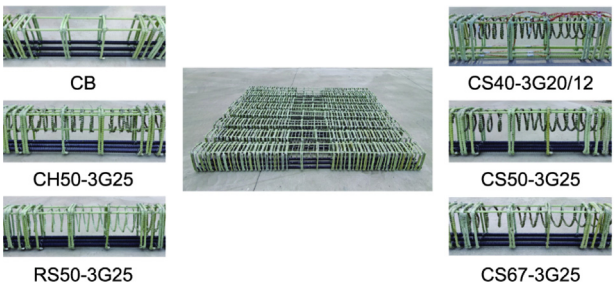

Fig. 2. FRP reinforcement cages of some of the test beams.

using a pultrusion technique with a custom-designed mold to achieve predefined shapes and dimensions.

2.3. Setup and instrumentation for the beam tests

All beam specimens were tested under two-point loading (i.e., four-point bending) with a distance of 600 mm (the pure bending region) between the two loading points. The load was applied using a 1000 kN capacity servo-controlled actuator (Hangzhou Popwil Instrument Co., Ltd., China), as shown in Fig. 4. The loading process consisted of three stages: a load-control stage initially at 3 kN increments before the cracking of the beam bottom surface and then at 10 kN increments until the appearance of concrete cover spalling near the top surface of the beam, followed by a displacement-control stage in increments of 1 mm until the complete failure of the beam. Prior to testing, the beams were painted white to facilitate clear observation of crack development. The vertical deflections of the beams were measured using five linear variable differential transformers (LVDTs; Liyang City Instrument and Meter Plant, China) located at critical positions (beam supports, mid-span, and loading points). Furthermore, 14 strain gauges (Zhejiang Huangyan Testing Apparatus Factory, China) with a gauge length of 5 mm were attached to the longitudinal FRP bars and spiral/hoops at the mid-span and one of the loading points of each FRP-CZC beam to monitor the FRP strain development. Nine strain gauges with a gauge length of 100 mm were installed at the mid-span over the beam height and on the top and bottom surfaces of the beam, as shown in Fig. 4(b). For the CB, the arrangement of strain gauges was similar, except for the compression zone FRP spiral/hoops, which did not exist in the CB.

Please cite this article as: S.-S. Zhang, X.-B. Hu and J.-G. Teng, Imparting Ductility to FRP-Reinforced Concrete Beams Through Compression Zone Confinement, Engineering, https://doi.org/10.1016/j.eng.2026.04.012

Table 1
Details of test beams.

Beam specimen	Tension GFRP reinforcement		GFRP stirrup in shear spans	GFRP confinement in the compression zone				$\frac{\rho_f}{\rho_{con}}$
	Bars	ρ_f (%)		d_s(mm)	s (mm)	ρ_w(%)	Configuration	
CB	3G25	2.88	G12@50	–	–	–	–	3.13
CS40-3G25	3G25	2.88	G12@50	9	40	5.17	CS	3.13
CS50-3G25	3G25	2.88	G12@50	9	50	4.14	CS	3.13
CS67-3G25	3G25	2.88	G12@50	9	67	3.09	CS	3.13
CS40-3G20/12	2G20 + 1G12	1.44	G12@50	9	40	5.17	CS	1.50
CS40-3G20	3G20	1.83	G12@50	9	40	5.17	CS	1.91
RS50-3G25	3G25	2.88	G12@50	9	50	4.20	RS	3.13
CH50-3G25	3G25	2.88	G12@50	9	50	4.14	CH	3.13

ρ_f : longitudinal tension FRP reinforcement ratio; d_s : nominal bar diameter of spiral; s: pitch or spacing of spiral/hoops; ρ_w : volumetric ratio of FRP spiral/hoops; ρ_{con} : balanced tension FRP reinforcement ratio of a corresponding FRP-RC beam without FRP confinement in the compression zone [33].

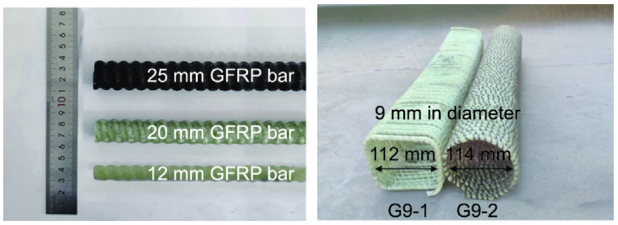

Fig. 3. GFRP bars used in the test beams. (a) Longitudinal/shear GFRP bars; (b) GFRP spirals (G9-1 and G9-2).

3. Experimental results

3.1. Failure mode

The failure modes of all the test beams are shown in Figs. 5–8. Control specimen CB failed in a brittle manner because of the compressive crushing of the top surface/top concrete cover. This top-surface compression failure (Fig. 5), denoted by "TC" hereafter, is the typical flexural failure mode of over-reinforced FRP-RC beams [37,38]. In contrast, the FRP-CZC beams failed in a more ductile manner, in accordance with design expectations. The FRP-CZC beams exhibited similar failure processes. With an increasing load, spalling of the top concrete cover occurred first, accompanied by a temporary drop in the applied load. However, owing to the FRP confinement effect on the compressive concrete, the beams were capable of sustaining an increasing load until the occurrence of ultimate failure, at which the load suddenly dropped by a large amount. The failure modes of FRP-CZC beams are preferable to that of the control specimen because the former are more gradual and less catastrophic, exhibiting substantially higher deformability/-ductility. The development of cracks in the test beams was recorded during the loading process. The first crack always occurred within the pure bending region, and several flexural and shear cracks appeared in the pure bending region and the two shear spans, respectively, as the load further increased. Meanwhile, the cracks in the shear spans gradually propagated toward the loading points with increasing load owing to the combination of flexural and shear stresses. After the load reached approximately 70% of the peak load, the number of cracks almost stopped increasing; instead, the existing cracks continued to deepen and widen.

The test observations indicated that three types of failure modes occurred in the FRP-CZC beams: ① Specimens CS40-3G25, CS50-3G25, CS67-3G25, and RS50-3G25 failed by the rupture of FRP spiral, followed by the compressive crushing of the confined concrete core (hereafter referred to as "RFS + CC" for simplicity), as shown in Fig. 6; ② Specimen CH50-3G25 failed by slippage between the two ends of the FRP hoop, followed by the compressive crushing of confined concrete core (hereinafter referred to as "SFH + CC" for simplicity), as shown in Fig. 7; and ③ specimens CS40-3G20/12 and CS40-3G20 failed by the rupture of longitudinal tension FRP bars (hereinafter referred to as "RT" for simplicity), as shown in Fig. 8. The FRP spiral in the beam experiencing RT failure did not rupture, and the integrity of the confined concrete core was maintained without penetrating cracks, indicating that the FRP confinement was not fully activated. After unloading, the damaged FRP-CZC beams with the first two failure modes almost recovered their original shapes owing to the linear elastic nature of FRP bars.

3.2. Load–deflection responses

The total load versus mid-span deflection curves of all the test beams are shown in Fig. 9(a). The control specimen showed classical bilinear characteristics, and the load quickly decreased after the compressive crushing of the top concrete of the beam. The FRP-CZC specimens exhibited not only an apparent yield plateau similar to that of conventional steel-RC beams but also an increase in the load and deformation capacities over the CB. This observation indicates that FRP confinement can increase both the compressive

Table 2
Material properties of GFRP bars.

Bar specimen	Nominal diameter[a] (mm)	Immersion diameter[b] (mm)	Elastic modulus[c] (GPa)	Tensile strength[c] (MPa)	Ultimate tensile strain[c] (%)	Surface configuration
G9-1	9	8.7	45.7	930	2.03	Spirally wrapped
G9-2	9	8.3	51.1	1114	2.18	Spirally wrapped
G12	12	11.5	44.5	767	1.72	Deep-ribbed
G20	20	19.0	44.3	714	1.61	Deep-ribbed
G25	25	24.0	45.5	738	1.62	Deep-ribbed

[a] Provided by the manufacturer.
[b] Determined from immersion test [36].
[c] Calculated based on the nominal diameter.

Please cite this article as: S.-S. Zhang, X.-B. Hu and J.-G. Teng, Imparting Ductility to FRP-Reinforced Concrete Beams Through Compression Zone Confinement, Engineering, https://doi.org/10.1016/j.eng.2026.04.012

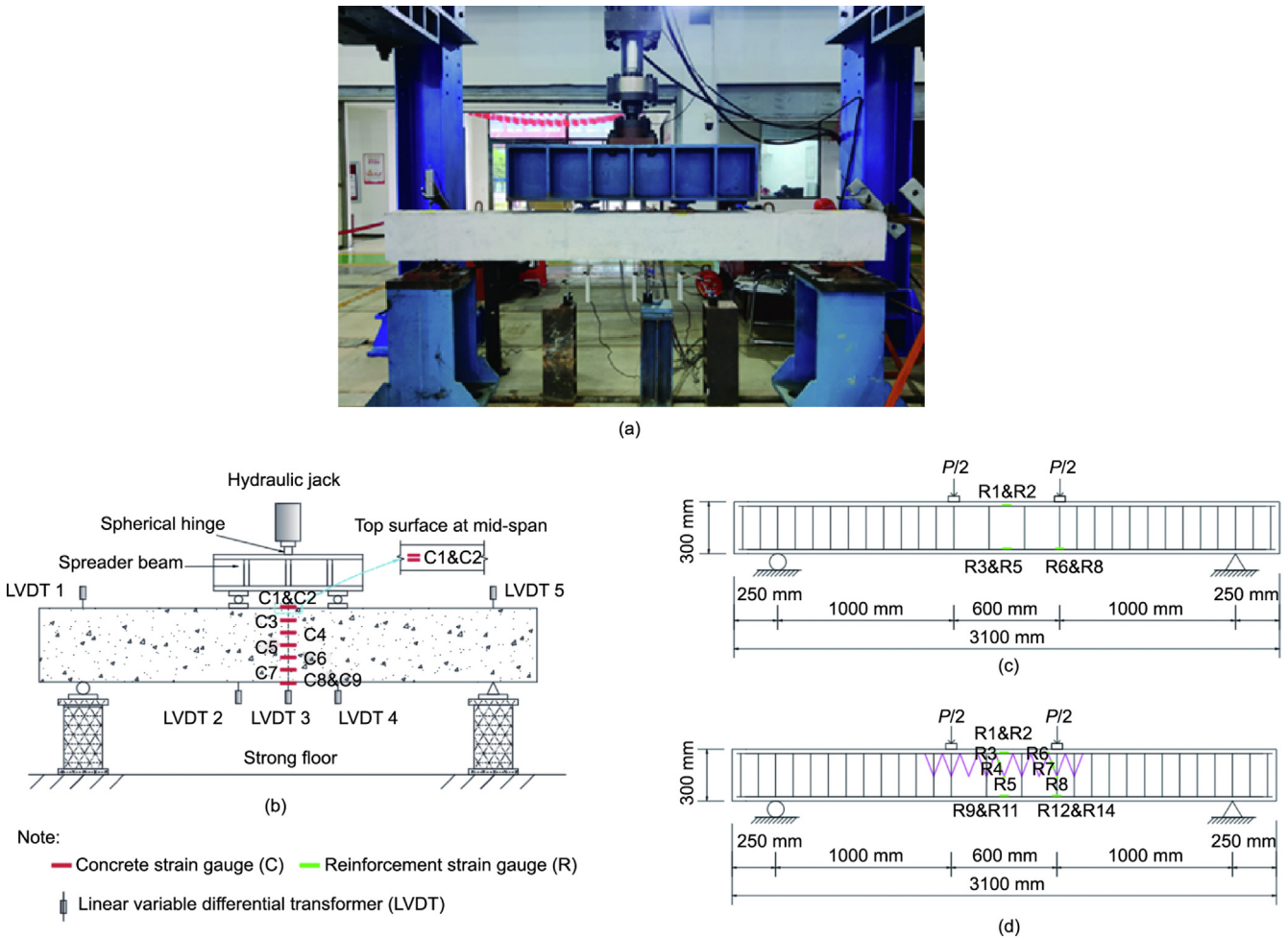

Fig. 4. Test setup and instrumentation. (a) Test setup; (b) LVDTs and concrete strain gauges; (c) strain gauges on FRP bars in the CB; (d) strain gauges on FRP bars in the FRP-CZC beams. *P* represent the corresponding total applied load.

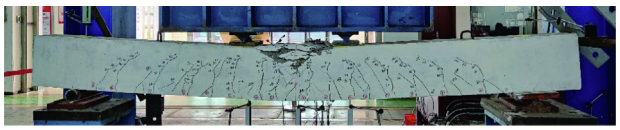

Fig. 5. TC failure of the CB.

strength and deformation capacity of the confined compressive concrete, resulting in an enhancement in the ductility of the beam. The stiffness of the FRP-CZC beams with the same longitudinal tension FRP bars did not vary significantly with the FRP confinement configuration before the compressive spalling of the top concrete cover. Subsequently, the FRP-CZC beams first experienced a slight decrease in load owing to the spalling of the top concrete cover. Soon after, the passive FRP confining effect on the compressive concrete core was activated by the dilation of the FRP-confined concrete, and then progressively increased as the load further increased. Once the FRP spiral/hoops ruptured, leading to the crushing of the compressive concrete core, the load-carrying capability of the FRP-CZC beam decreased rapidly, signifying the final failure of the beam. In Fig. 9, the marked point on each curve with the associated failure phenomenon identified corresponds to the final failure of the beam, beyond which an abrupt drop in the load-bearing capacity occurs.

Three typical simplified load–deflection curves for the FRP-CZC beams are shown in Fig. 10. In these curves, the symbols δ and P represent the mid-span deflection and the corresponding total applied load, respectively. The subscripts are defined as follows: "cr" denotes bottom concrete cover cracking (Point 1); "p1" denotes compressive spalling of the top concrete cover (Point 2); "p2" denotes the activation of the FRP confinement effect (Point 3); and "u" denotes the ultimate failure of the beam (Point 4). The curves generally consist of four portions in sequence of appearance: ① the linear-elastic portion: The load increases linearly with the deflection until the bottom concrete cover cracking point (δ_{cr}, P_{cr}) is reached. In this study, the first concrete cracking in the FRP-CZC beams occurred at a load level of 15–21 kN. ② The linear post-cracking portion: After concrete cracking, the load continues to increase with the deflection at a slope smaller than that of the first portion until the compressive spalling of the top concrete cover (δ_{p1}, P_{p1}). ③ The load-reduction portion: After the spalling of top concrete cover, the FRP-CZC specimens experienced a load decrease of 5.6%–12.0% until the activation of the FRP confinement effect (δ_{p2}, P_{p2}). ④ The confinement-effective portion: After the activation of the FRP confinement effect, the load keeps increasing or decreasing along a nearly linear path as the deflection increases at a small slope until the complete failure of the beam (δ_u, P_u). Note that the load–deflection curves in the fourth segment can be ascending, horizontal, or descending, depending on the level of

Please cite this article as: S.-S. Zhang, X.-B. Hu and J.-G. Teng, Imparting Ductility to FRP-Reinforced Concrete Beams Through Compression Zone Confinement, Engineering, https://doi.org/10.1016/j.eng.2026.04.012

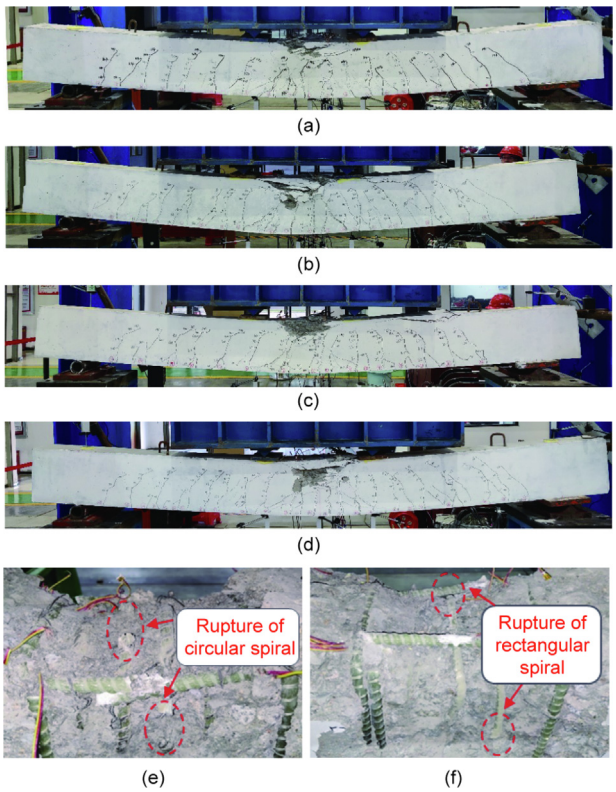

Fig. 6. Rupture of FRP spiral followed by the compressive crushing of the confined concrete core (RFS + CC) failure in FRP-CZC beams. (a) Side view of CS40-3G25; (b) side view of CS50-3G25; (c) side view of CS67-3G25; (d) side view of RS50-3G25; (e) close-up view of CS40-3G25; (f) close-up view of RS50-3G25.

FRP confinement, which is related to the pitch (i.e., volumetric ratio) and configuration of the FRP spiral. By considering the level of confinement and the associated slope of the fourth portion of the load–deflection curve, FRP-CZC beams may be classified into "heavily confined beams" with an ascending fourth portion, "moderately confined beams" with a horizontal fourth portion, and "weakly confined beams" with a descending fourth portion, as shown in Fig. 10. Fig. 9(d) shows that one of the FRP-CZC beams (Specimen RS50-3G25) exhibited approximately moderately confined beam behavior. The other FRP-CZC beams exhibited heavily confined beam behavior, as the FRP confinement led to a significantly ascending fourth portion. A small load fluctuation, accompanied by a small explosive sound during the test, was noted in the fourth portion of the load–deflection curve for some of the beams owing to the rupture of the compressive FRP bars; however, this was soon followed by a rebound phase arising from the increasing activation of the FRP confinement effect. Note that the load decrease caused by the spalling of the top concrete cover has an insignificant effect on the overall behavior of FRP-CZC beams, as such a decrease is usually small when practical concrete cover thicknesses are adopted. Meanwhile, the spalling of top concrete cover is not the ultimate state of FRP-CZC beams, but can be treated as a sign of beam damage and can be repaired if necessary.

The key test results for all beam specimens are summarized in Table 3. It is expected that the four key points (δ_{cr}, P_{cr}), (δ_{p1}, P_{p1}), (δ_{p2}, P_{p2}), and (δ_u, P_u) generally define the load–deflection response of an FRP-CZC beam. As shown in Fig. 10, the ultimate states for the control and FRP-CZC beams correspond to Points 2 and 4, respectively, where the load suddenly drops by a large amount. As provided in Table 3, the heavily confined beams with an ascending fourth portion of the load–deflection response achieved a substantial enhancement in both the ultimate deflection and load-carrying capacity.

3.2.1. Effect of FRP spiral pitch

The load–deflection curves of FRP-CZC beams with different FRP spiral pitches are compared in Fig. 9(b). Specimens CS40-3G25, CS50-3G25, and CS67-3G25, with spiral pitches of 40, 50, and 67 mm, respectively, together with the control specimen CB, are included. The figure indicates that the effect of spiral pitch on the load–deflection curve is less evident before the compressive spalling of top concrete cover. After the spalling of the top concrete cover and FRP confinement activation, the load of a beam with a smaller spiral pitch increases more rapidly with the deflection,

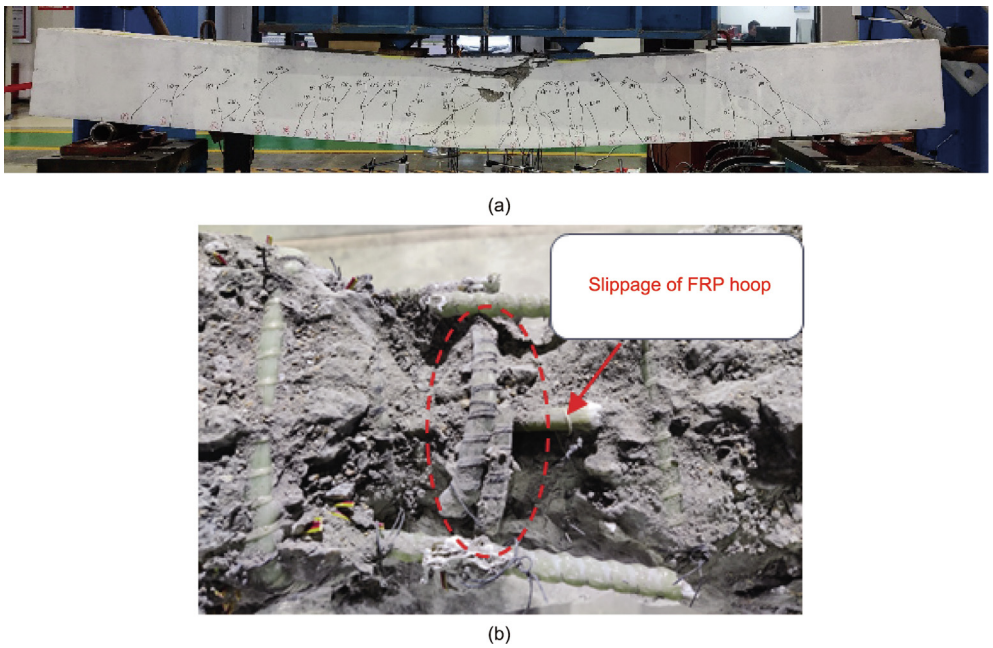

Fig. 7. Slippage between the two ends of the FRP hoop followed by the compressive crushing of confined concrete core (SFH + CC) failure in beam CH50-3G25. (a) Overall view; (b) close-up view.

Please cite this article as: S.-S. Zhang, X.-B. Hu and J.-G. Teng, Imparting Ductility to FRP-Reinforced Concrete Beams Through Compression Zone Confinement, Engineering, https://doi.org/10.1016/j.eng.2026.04.012

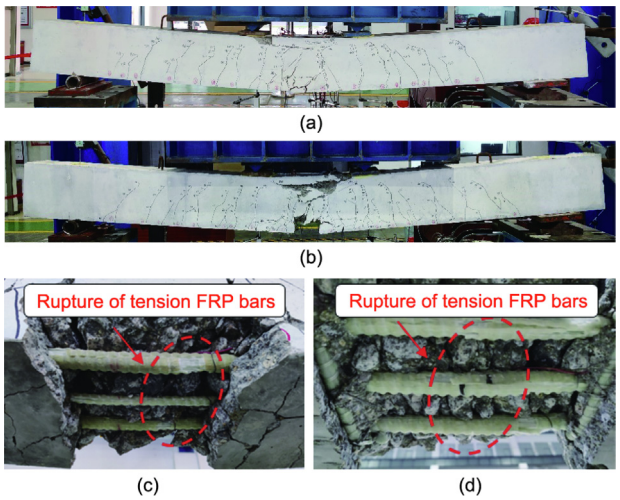

Fig. 8. Rupture of longitudinal tension (RT) failure in FRP-CZC beams. (a) Side view of CS40-3G20/12; (b) side view of CS40-3G20; (c) close-up view of CS40-3G20/12; (d) close-up view of CS40-3G20.

leading to a higher load and larger deflection at beam failure. The ultimate load and deflection of Specimen CS40-3G25 are higher than those of Specimen CS67-3G25 by 19.8% and 25.7%, respectively.

3.2.2. Effect of tension FRP reinforcement ratio

The load–deflection responses of the beams with different longitudinal tension FRP reinforcement ratios are shown in Fig. 9(c). Specifically, Specimens CS40-3G25, CS40-3G20, and CS40-3G20/12 (with longitudinal tension FRP reinforcement ratios of 2.88%, 1.83%, and 1.44%, respectively), together with the control Specimen CB (with a longitudinal tension FRP reinforcement ratio of 2.88%), are compared. As shown in Fig. 9(c), the longitudinal tension FRP reinforcement ratio has a significant effect on the load–deflection curve of the beam. A higher FRP reinforcement ratio results in a greater flexural stiffness and a higher load at the spalling of top concrete cover; for instance, the P_{p1} of Specimen CS40-3G25 is 41.3% higher than that of Specimen CS40-3G20/12. After the compressive spalling of top concrete cover, the beam with a higher longitudinal tension FRP reinforcement ratio reached a higher ultimate load and corresponding deflection at beam failure. Increasing the longitudinal tension FRP reinforcement ratio from 1.44% to 2.88% (CS40-3G20/12 versus CS40-3G25) resulted in enhancements of ultimate load and corresponding mid-span deflection by 45.5% and 35.3%, respectively. Meanwhile, the three FRP-CZC beams did not exhibit a considerable difference in the slope of the fourth portion of the load–deflection curve, indicating that the flexural stiffness of this portion is mainly controlled by the configuration/level of FRP confinement. Note that the specimens with a low longitudinal reinforcement ratio were designed for comparison purposes. In the real design of this novel FRP-CZC beam, the beam should be over-reinforced to fully activate the FRP confinement, and thus achieve a higher level of ductility.

3.2.3. Effect of FRP confinement configuration

The load–deflection responses of the FRP-CZC beams with different FRP confinement configurations are compared in Fig. 9(d). Specifically, Specimens CS50-3G25, RS50-3G25, and CH50-3G25 (with a continuous circular FRP spiral, a continuous rectangular FRP spiral, and discrete circular FRP hoops, respectively), together with the control Specimen CB, are compared. As shown in

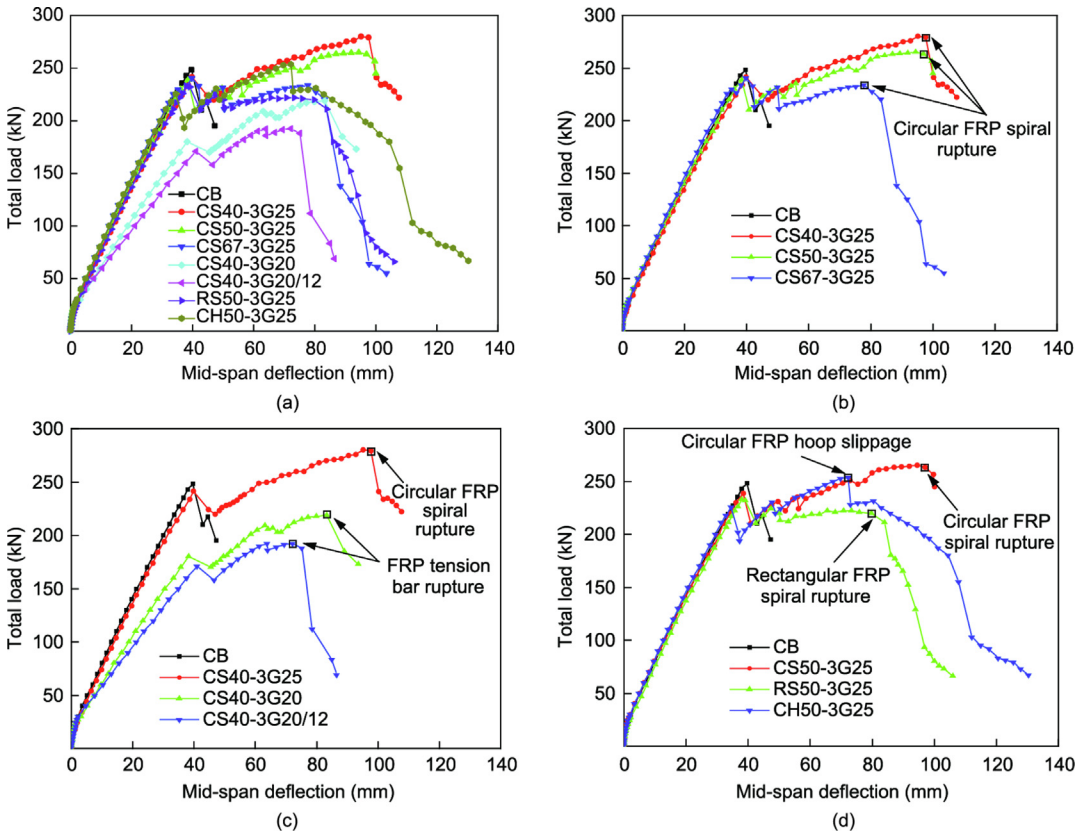

Fig. 9. Total load–deflection curves of all test beams. (a) All test beams; (b) effect of FRP spiral pitch; (c) effect of tension FRP reinforcement ratio; (d) effect of FRP confinement configuration.

Please cite this article as: S.-S. Zhang, X.-B. Hu and J.-G. Teng, Imparting Ductility to FRP-Reinforced Concrete Beams Through Compression Zone Confinement, Engineering, https://doi.org/10.1016/j.eng.2026.04.012

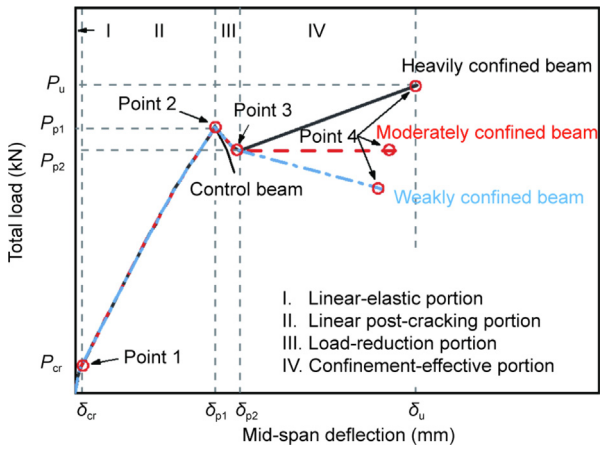

Fig. 10. Typical simplified load–deflection curve of FRP-CZC beams.

Fig. 9(d), the specimens with a circular FRP spiral (i.e., Specimen CS50-3G25) showed the best performance in terms of flexural capacity and ductility; the specimen with discrete circular hoops (i.e., Specimen CH50-3G25) had a similar behavior to that with a circular FRP spiral (i.e., Specimen CS50-3G25) before the occurrence of relative slippage between the two ends in the overlapping zone of the FRP hoop and thus the debonding between FRP hoop ends and concrete, after which the load dropped suddenly and then decreased gradually; the specimen with a rectangular FRP spiral (i.e., Specimen RS50-3G25) gained the least from FRP confinement as the fourth portion is almost horizontal, indicating that a rectangular FRP spiral offered much less confinement to the concrete than a circular spiral. Moreover, a 67 mm pitch circular FRP spiral (i.e., Specimen CS67-3G25) was also found to be much more effective in enhancing the flexural performance of the beam than a 50 mm pitch rectangular FRP spiral (i.e., Specimen RS50-3G25), as shown in Fig. 9(a).

3.3. Strain analysis

Fig. 11 shows the strain distributions of the four typical beams down the mid-span beam height for different load levels. Note that Fig. 11 shows the strain distributions before compressive spalling of the top concrete cover, after which most of the strain gauges on the FRP bars and concrete surface failed to function. As shown in Fig. 11, the strain distributions down the beam height are approximately linear, indicating that the plane section assumption is applicable to these FRP-CZC beams before spalling of the top concrete cover.

The neutral-axis depths at the mid-span of all specimens before the spalling of top concrete cover are shown in Fig. 12. These neutral-axis depths were obtained from the strain distributions (based on the strain gauges on the top concrete surface and longitudinal tension FRP bars) down the beam height [39,40]. As shown in Fig. 12, a higher longitudinal tension FRP reinforcement ratio leads to a larger neutral-axis depth ratio (c/h_0, where c is the neutral-axis depth), with the value of Specimen CS40-3G25 being 32.7% higher than that of Specimen CS40-3G20/12. The figure further shows the variation in the neutral-axis depth with an increasing load: The neutral axis is initially below the mid-height of the beam cross-section but quickly moves upward (i.e., the neutral-axis depth quickly decreases) after the tensile cracking of bottom concrete cover and remains virtually constant thereafter. In Fig. 12, the neutral axes of the FRP-CZC specimens are above the bottom edge of the FRP spiral/hoops, indicating that part of the confined concrete core was under tension. For FRP-CZC beams, a large neutral-axis depth (i.e., a larger compression zone) is preferable because FRP confinement is more effective when the entire confined concrete core is under compression. Increasing the longitudinal-tension FRP reinforcement ratio can lower the position of the neutral axis on the beam cross-section, leading to a larger compressive area for the confined concrete core.

Fig. 13 shows the relationship between the load and the hoop strains of the FRP spiral/hoop at the mid-span for the three specimens. Strain gauges R3, R4, and R5 were installed at the top, mid-height, and bottom of the FRP spiral/hoop, respectively, as shown in Fig. 4(d). As shown in Fig. 13, the strains of the FRP spiral/hoop remained at a relatively low level before the spalling of the top concrete cover, after which rapid increases in these strains occurred.

3.4. Ductility and deformability

Two approaches were examined to assess the flexural ductility of FRP-RC beams.

3.4.1. Deformation-based approach

To evaluate the flexural ductility of FRP-CZC beams, the classic deformation-based approach for conventional steel-RC beams was first adopted [41], as given in Eq. (1). To determine the equivalent yield point on the load–deflection curve of FRP-CZC beams, the equivalent elasto-plastic energy absorption concept [42,43] was adopted in the present study (leading to ductility index μ_{d1}), as shown in Fig. 14. Furthermore, the first peak point on the load–deflection curve (i.e., Point 2 in Fig. 10) was chosen as an alternative yield point to evaluate another ductility index (referred to as μ_{d2}) for comparison purposes.

Table 3
Key test results.

Beam specimen	First cracking		Spalling of top concrete cover		Activation of FRP confinement effect		Ultimate state		$\varepsilon_{c,max}$ (με)	Failure mode
	P_{cr} (kN)	δ_{cr} (mm)	P_{p1} (kN)	δ_{p1} (mm)	P_{p2} (kN)	δ_{p2} (mm)	P_u (kN)	δ_u (mm)		
CB	18.0	0.83	248.3	39.61	–	–	248.3	39.61	3796	TC
CS40-3G25	18.0	1.11	241.6	39.83	220.0	46.94	280.0	97.68	3780	RFS + CC
CS50-3G25	21.0	0.78	238.7	38.43	210.0	40.78	263.3	96.96	3768	RFS + CC
CS67-3G25	18.0	0.80	240.5	39.74	213.0	42.49	233.8	77.72	3731	RFS + CC
CS40-3G20/12	15.0	0.90	171.0	41.04	158.0	46.58	192.5	72.19	2721	RT
CS40-3G20	21.0	0.97	180.0	38.19	170.0	45.47	219.0	83.23	3110	RT
RS50-3G25	18.0	1.01	233.0	37.84	210.0	42.52	220.0	79.75	3664	RFS + CC
CH50-3G25	21.0	0.95	225.6	34.46	193.5	37.24	253.5	72.21	3130	SFH + CC

$\varepsilon_{c,max}$ is the recorded maximum concrete compressive strain at the top surface of the beam.

Please cite this article as: S.-S. Zhang, X.-B. Hu and J.-G. Teng, Imparting Ductility to FRP-Reinforced Concrete Beams Through Compression Zone Confinement, Engineering, https://doi.org/10.1016/j.eng.2026.04.012

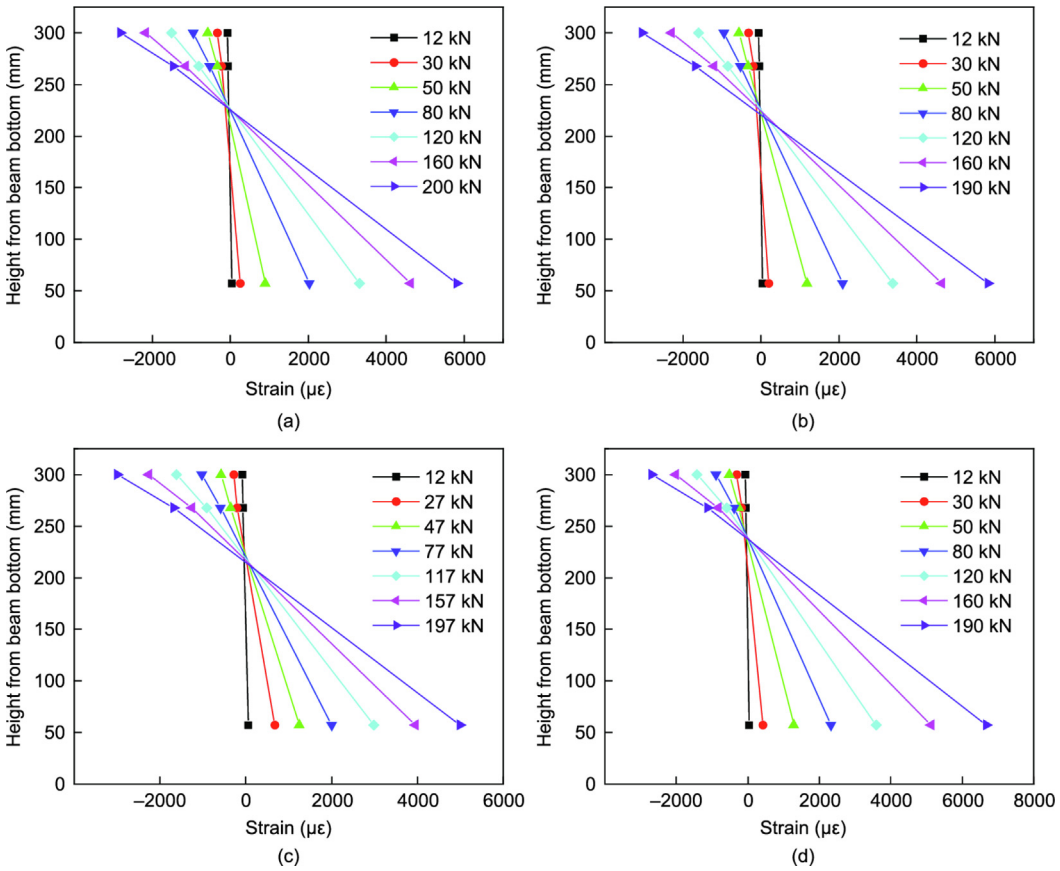

Fig. 11. Strain distributions down the mid-span height. (a) CB; (b) CS50-3G25; (c) RS50-3G25; (d) CH50-3G25.

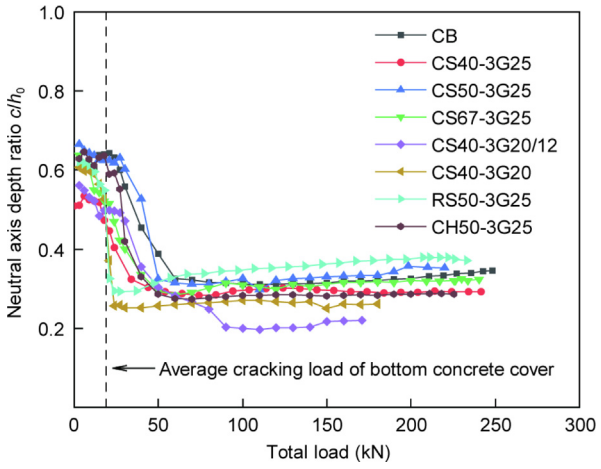

Fig. 12. Variation of neutral-axis depth with load.

$$\mu_d = \frac{\delta_u}{\delta_y} \tag{1}$$

where δ_u denotes the ultimate deflection; δ_y denotes the equivalent yield deflection, defined as Point 2 on a load–deflection curve of the type shown in Fig. 10 or determined using the energy equivalence method (Fig. 14).

3.4.2. Energy-based approach

The energy-based ductility index (μ_e, Eq. (2)), proposed by Naaman and Jeong [44] for FRP-RC beams, was adopted in the present study to evaluate the flexural ductility of FRP-CZC beams.

$$\mu_e = \frac{1}{2}\left(\frac{E_{tot}}{E_{el}} + 1\right) \tag{2}$$

where E_{tot} is the total energy (i.e., the area under the load–deflection curve up to the failure load) and E_{el} is the elastic energy, as shown in Fig. 15.

3.4.3. Discussions

The beam ductility index values calculated using the aforementioned methods are shown in Fig. 16. It can be seen from Fig. 16 that the ductility index values obtained from the energy-based method (i.e., μ_e) are the highest, and the values of the second ductility index (i.e., μ_{d2}) obtained from the deformation-based method are the lowest. Further, the ductility index values of FRP-CZC beams obtained using any of the above methods are considerably higher than those of the CB, indicating that FRP confinement of the compression zone can greatly improve the ductility of an FRP-CZC beam.

Moreover, Fig. 16 shows that: ① The use of a circular FRP spiral as the confining device leads to a higher level of ductility than the use of a rectangular FRP spiral or discrete FRP hoops; ② a smaller pitch (i.e., a larger volumetric ratio) of the FRP spiral leads to a higher confinement level to the compressive concrete and hence a higher level of ductility of the beam; and ③ a larger longitudinal tension FRP reinforcement ratio leads to a higher level of ductility for the beam as the rupture of tension FRP bars can be prevented or delayed. Note that the incorporation of FRP spirals into the compression zone can significantly improve the ductility of FRP-RC beams with an acceptable cost increase. For example, the energy-based ductility index of Specimen CS40-3G25 was about 2.5 times that of the control specimen, but the increase in FRP cost was only 7.1% approximately.

Please cite this article as: S.-S. Zhang, X.-B. Hu and J.-G. Teng, Imparting Ductility to FRP-Reinforced Concrete Beams Through Compression Zone Confinement, Engineering, https://doi.org/10.1016/j.eng.2026.04.012

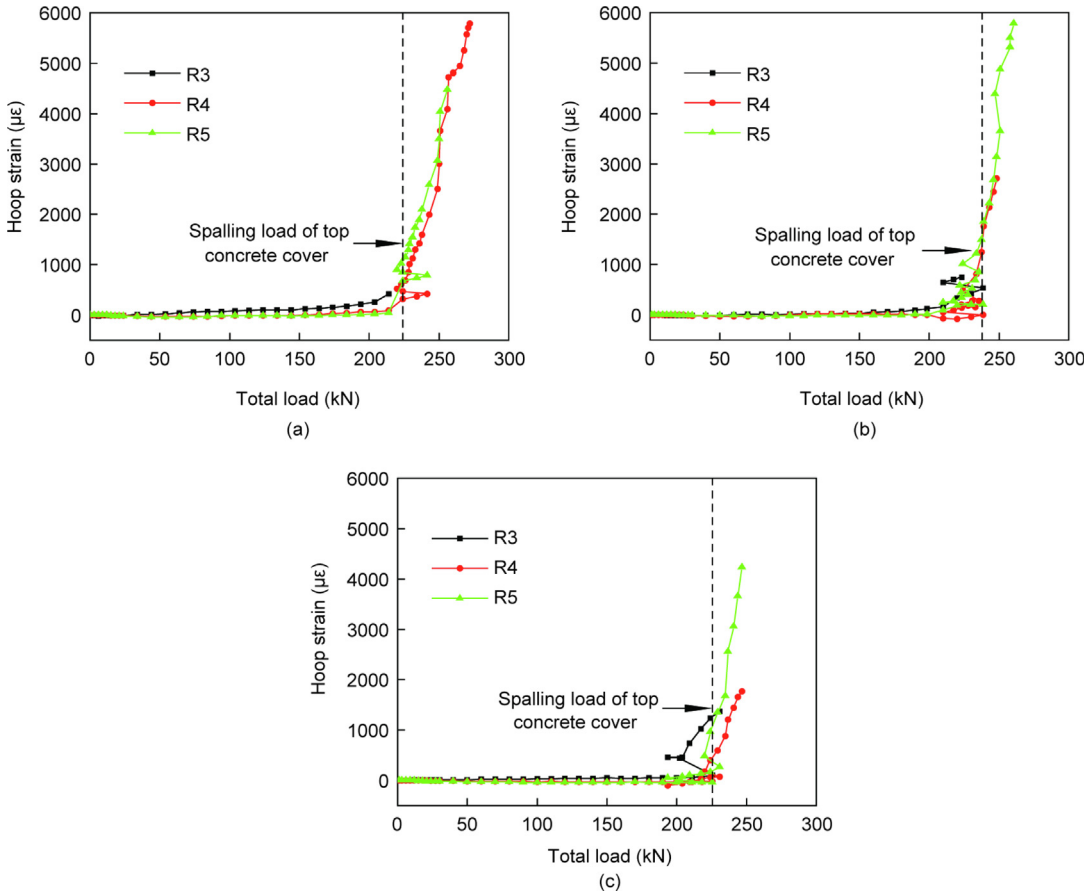

Fig. 13. Variation of hoop strains in FRP spiral/hoop with load. (a) CS40-3G25; (b) CS50-3G25; (c) CH50-3G25.

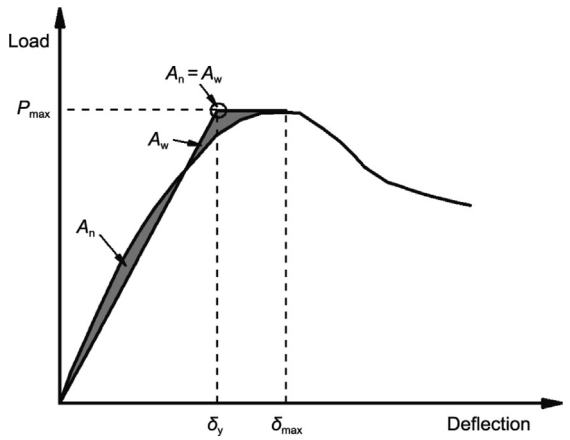

Fig. 14. Definition of the equivalent yield deflection. P_{max} and δ_{max} represent the peak load and the corresponding deflection, respectively. The areas A_n and A_w, enclosed by the equivalent bi-linear response curve and the actual response curve, are equal.

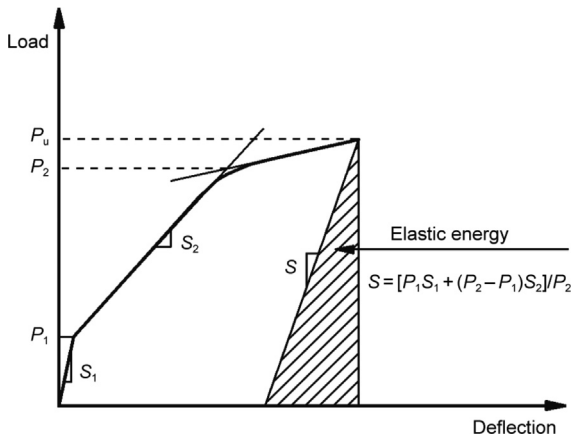

Fig. 15. Definition of energy-based ductility index. P_1, P_2, and P_u represent the characteristic loads on the curve, while S_1, S_2, and S denote the relevant slopes on the curve.

4. Numerical modeling

4.1. Proposed FE approach

4.1.1. FE mesh

A 3D nonlinear FE study was conducted on the test beams of the present study using the general-purpose software ABAQUS 6.14 (Dassault Systèmes, France) [45]. Owing to the lack of reliable axial stress–strain models for concrete confined with rectangular FRP spirals or discrete FRP hoops, the FE analyses mainly focused on the CZC beams with a circular FRP spiral in the compression zone (i.e., Specimens CS40-3G25, CS50-3G25, CS67-3G25, CS40-3G20/12, and CS40-3G20), together with the control specimen CB. For circular FRP spiral confined-concrete (FSCC), the model proposed by Zeng et al. [46], which has been shown to be able to predict the axial stress-strain response of FSCC well, was adopted in the present study. Fig. 17 shows the boundary conditions, element types, and loading scheme. Before the FE meshing process, a partition of the beam was made to separate the FRP spiral-confined concrete core from the unconfined concrete region to facilitate the assignment of different material properties. The

Please cite this article as: S.-S. Zhang, X.-B. Hu and J.-G. Teng, Imparting Ductility to FRP-Reinforced Concrete Beams Through Compression Zone Confinement, Engineering, https://doi.org/10.1016/j.eng.2026.04.012

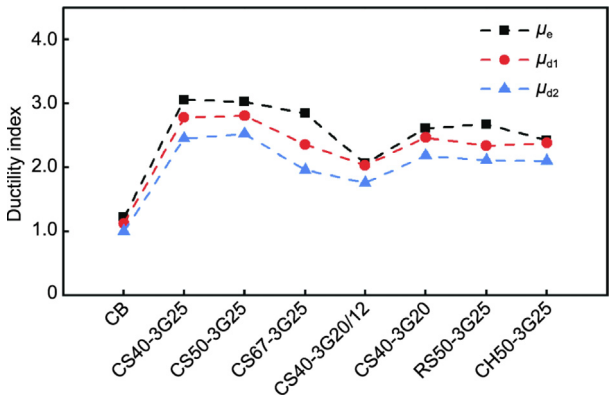

Fig. 16. Ductility indexes.

structured meshing technique available in ABAQUS [45] using a proper section partitioning scheme was employed to mesh the beam section. Through a mesh sensitivity analysis, the approximate global element size [45] was determined to be 16 mm (the approximate global element size represents the fineness level of meshing, and the real element size may be slightly different from it depending on the geometry) and the FE mesh of the beam is shown in Fig. 17. The concrete, steel loading plates, and support blocks were modeled using 8-node solid reduced integration elements (C3D8R). The FRP bars were represented using 2-node linear truss elements (T3D2). A perfect bond was assumed between FRP bars and adjacent concrete by using the "embedded" constraint available in ABAQUS. A tie contact was defined between the top loading plates or bottom support blocks and the corresponding beam surfaces. The centroid of the top surface of each loading plate or the bottom surface of each support block was selected as the reference point and coupled with the corresponding surface. External loading was applied to the two reference points on the loading plates using the displacement control method. Based on the loading scheme, the reference point of the left support block was designated as a pin support, whereas the reference point of the right support was configured as a roller support.

4.1.2. Constitutive modeling of unconfined concrete

The concrete damaged plasticity (CDP) model available in ABAQUS [45] was employed to simulate the concrete in the FE analysis. The relevant parameters in the CDP model were defined as follows: The dilation angle was 30°, the flow potential eccentricity was 0.1, the ratio of initial equibiaxial compressive yield stress to initial uniaxial compressive yield stress was 1.16, and the ratio of the second stress invariant on the tensile meridian to that on the compressive meridian was 0.667 [45]. Following the Chinese national standard GB 50010–2010 [47], the axial compressive and tensile stress–strain relationships of the unconfined normal concrete were defined using Eqs. (3) and (4), respectively, with typical curves illustrated in Fig. 18.

$$\sigma_c = E_c\varepsilon_c \begin{cases} \dfrac{\dfrac{f_{co}}{E_c\varepsilon_{co}-f_{co}}}{\dfrac{E_c\varepsilon_{co}}{E_c\varepsilon_{co}-f_{co}}-1+\left(\dfrac{\varepsilon_c}{\varepsilon_{co}}\right)^{\frac{E_c\varepsilon_{co}}{E_c\varepsilon_{co}-f_{co}}}} & \varepsilon_c \le \varepsilon_{co} \\ \dfrac{\dfrac{f_{co}}{E_c\varepsilon_{co}}}{\alpha_c\left(\dfrac{\varepsilon_c}{\varepsilon_{co}}-1\right)^2+\dfrac{\varepsilon_c}{\varepsilon_{co}}} & \varepsilon_c > \varepsilon_{co} \end{cases} \tag{3}$$

$$\sigma_t = E_c\varepsilon_t \begin{cases} \left(\dfrac{f_{to}}{E_c\varepsilon_{to}}\right)\left(1.2-0.2\left(\dfrac{\varepsilon_t}{\varepsilon_{to}}\right)^5\right) & \varepsilon_t \le \varepsilon_{to} \\ \dfrac{\dfrac{f_{to}}{E_c\varepsilon_{to}}}{\alpha_t\left(\dfrac{\varepsilon_t}{\varepsilon_{to}}-1\right)^{1.7}+\dfrac{\varepsilon_t}{\varepsilon_{to}}} & \varepsilon_t > \varepsilon_{to} \end{cases} \tag{4}$$

where σ_c and ε_c denote the compressive stress and strain of concrete, while σ_t and ε_t denote the tensile stress and strain of concrete, respectively; f_{co} and ε_{co} represent the peak compressive stress and corresponding strain of concrete, while f_{to} and ε_{to} represent the peak tensile stress and corresponding strain of concrete, respectively; E_c is the elastic modulus of concrete (in MPa), calculated as $E_c = 4730\sqrt{f_{co}}$ according to ACI-318 [48]; α_c and α_t are factors governing the descending parts of the curves [46]. In addition, the following damage model was employed to define the damage evolution of the concrete [49]:

$$d_k = 1 - \frac{\sigma_k}{\sigma_{ko}} \tag{5}$$

In Eq. (5), the subscript "k" refers to the type of stress, with "c" denoting compression and "t" denoting tension, respectively; σ_k is the axial stress; and σ_{ko} is the peak stress.

4.1.3. Modeling of FRP spiral-confined concrete

The axial stress–strain relationship proposed by Zeng et al. [46] was adopted to define the compressive behavior of the FRP spiral-confined concrete core, as described by Eqs. (6)–(10) with the typical curves shown in Fig. 19.

$$\sigma_c = \begin{cases} E_c\varepsilon_c - \frac{(E_c-E_2)^2}{4f_{co}}\varepsilon_c^2 & (0 \le \varepsilon_c \le \varepsilon_{tr}) \\ \begin{cases} f_{co}+E_2\varepsilon_c & \rho_{Ke} \ge 0.033 \\ f_{co}-\frac{f_{co}-f_{cu}}{\varepsilon_{cu}-\varepsilon_{co}}(\varepsilon_c-\varepsilon_{co}) & \rho_{Ke} \ge 0.033 \end{cases} & (\varepsilon_{tr} \le \varepsilon_c \le \varepsilon_{cu}) \end{cases} \tag{6}$$

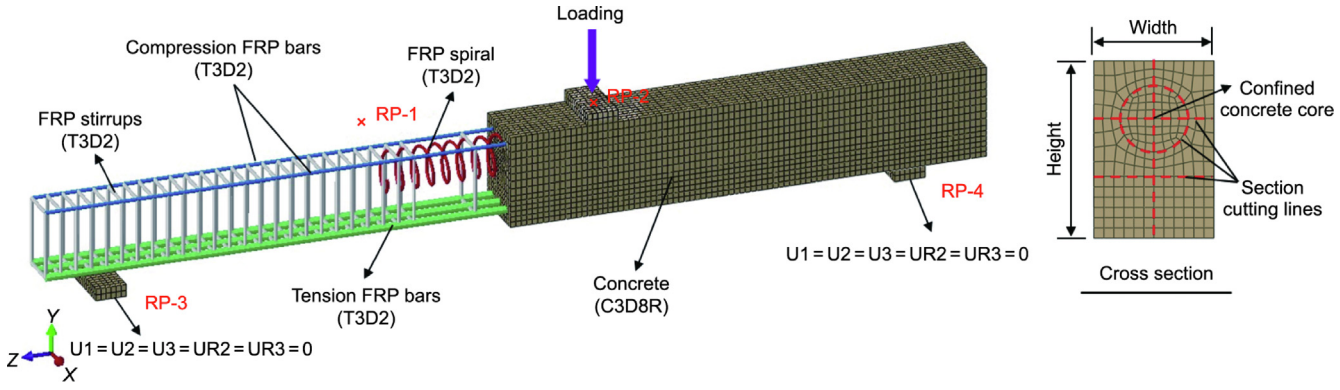

Fig. 17. Meshing, element types, and boundary conditions. RP-1 and RP-2 represent the reference points of the two loading plates; RP-3 and RP-4 represent the reference points of the two support blocks; U1, U2, U3, UR1, UR2, and UR3 represent the translational and rotational displacement components along directions 1, 2, and 3 in the global coordinate system, respectively. The red "×" marks indicate the positions of the reference points RP-1 and RP-2.

Please cite this article as: S.-S. Zhang, X.-B. Hu and J.-G. Teng, Imparting Ductility to FRP-Reinforced Concrete Beams Through Compression Zone Confinement, Engineering, https://doi.org/10.1016/j.eng.2026.04.012

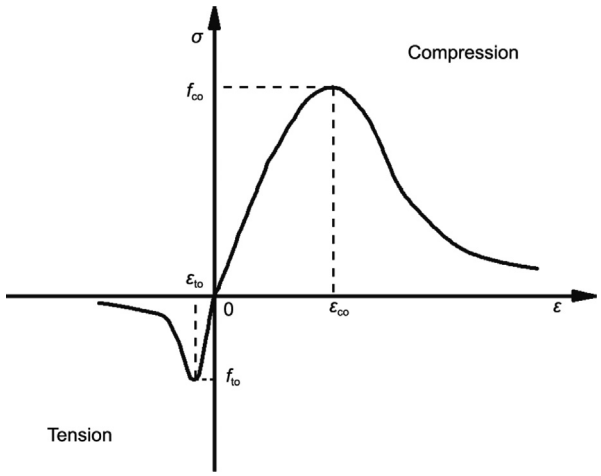

Fig. 18. Stress–strain curve for unconfined normal concrete.

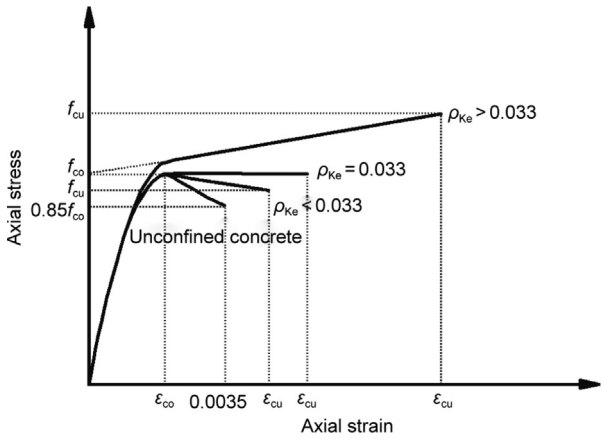

Fig. 19. Stress–strain curves for FRP spiral-confined concrete.

$$\frac{f_{cu}}{f_{co}} = 1.0 + 3.2(\rho_{Ke} - 0.033)\rho_{\varepsilon} \tag{7}$$

$$\frac{\varepsilon_{cu}}{\varepsilon_{co}} = 1.75 + 2.5\rho_{Ke}^{0.5}\rho_{\varepsilon}^{1.45} \tag{8}$$

$$E_2 = \frac{f_{cu} - f_{co}}{\varepsilon_{cu}} \tag{9}$$

$$\varepsilon_{tr} = \frac{2f_{co}}{E_c - E_2} \tag{10}$$

In the above equations, ρ_{Ke} and ρ_{ε} are the confinement stiffness ratio and strain ratio, respectively; f_{cu} is the ultimate compressive stress; ε_{cu} is the ultimate compressive strain; E_2 is the tangent modulus; and ε_{tr} is the transition strain.

4.1.4. Modeling of FRP reinforcement

A linear elastic stress–strain relationship was assigned to the FRP bars, including the tension bars, compression bars, stirrups, and confining spirals, as expressed by Eq. (11).

$$\sigma_f = \begin{cases} E_f\varepsilon_f & \varepsilon_f \le \varepsilon_{f,rup} \\ 0 & \varepsilon_f > \varepsilon_{f,rup} \end{cases} \tag{11}$$

In the above equation, σ_f and ε_f are the axial stress and strain of FRP bars, respectively; E_f is the elastic modulus of FRP bars; and $\varepsilon_{f,rup}$ is the rupture strain.

4.1.5. Dynamic simulation approach

The explicit dynamic analysis approach, proven to yield accurate predictions for quasi-static structural problems [50], was adopted in the present study. Based on the previous studies of the authors' group [51,52], the damping factor and loading time were respectively set to 1×10^{-6} and $50T_1$, respectively, where T_1 is the period of the fundamental vibration mode of the simulated specimen. For the damping scheme, a stiffness-proportional Rayleigh damping matrix $\boldsymbol{C} = \beta\boldsymbol{K}$ (β represents the damping factor defined in the FE model, and $\boldsymbol{K}$ is the stiffness matrix) was implemented.

4.2. FE results and comparisons

4.2.1. Ultimate loads

Fig. 20 and Table 4 compare the ultimate loads between the FE predictions and test results for the six specimens. The FE analyses yielded acceptable predictions for the test results, as indicated by the average, standard deviation (STD), and coefficient of variation (CoV) of the FE-to-test ultimate load ratios of 0.98, 0.050, and 0.0511, respectively. This agreement confirms the accuracy of the proposed FE approach for predicting the ultimate loads of FRP-CZC beams.

4.2.2. Failure modes

The failure modes of FRP-RC beams obtained from the FE simulations and the tests are compared in Figs. 21–23, from which it can be seen that the FE simulations demonstrated good agreement with the failure characteristics of the test beams, including top concrete damage, crack distributions, and FRP bar rupture. For the control specimen CB, the TC failure and crack patterns are well predicted, as shown in Fig. 21. The FRP-CZC beams with circular FRP spiral confinement exhibited two types of failure modes: ① rupture of the FRP spiral followed by crushing of the top confined concrete core (RFS + CC) and ② rupture of the FRP tension bar. In this study, two representative specimens (CS40-3G25 and CS40-3G20) were selected to demonstrate the performance of the proposed FE approach in predicting the failure modes and crack patterns of the FRP-CZC beams. The RFS + CC failure mode of Specimen CS40-3G25 was captured well by the proposed FE approach, featuring significant compressive damage near the top concrete at the mid-span of the beam, as shown in Fig. 22. The RT failure of Specimen CS40-3G20 was also closely captured by the proposed FE approach, featuring the tensile rupture of bottom FRP bars at beam failure, as shown in Fig. 23. The above comparisons indicate that the proposed FE approach can provide accurate predictions of the failure modes of the test beams.

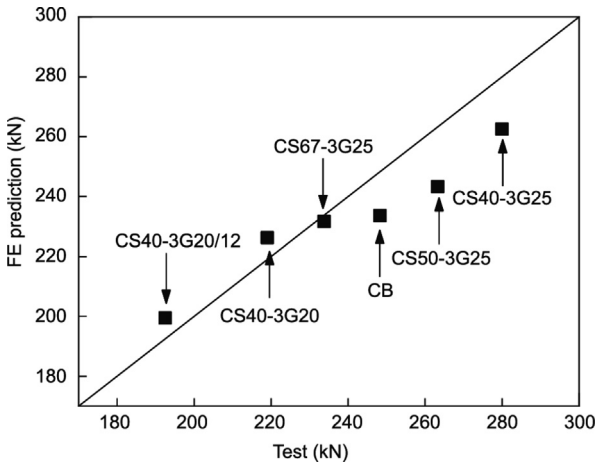

Fig. 20. Comparison of ultimate loads between FE analyses and tests.

Please cite this article as: S.-S. Zhang, X.-B. Hu and J.-G. Teng, Imparting Ductility to FRP-Reinforced Concrete Beams Through Compression Zone Confinement, Engineering, https://doi.org/10.1016/j.eng.2026.04.012

Table 4
FE and test ultimate loads.

Specimen	Test (kN)	FE prediction (kN)	FE-to-test ultimate load ratio
CB	248.3	233.6	0.94
CS40-3G25	280.0	262.5	0.94
CS50-3G25	263.3	243.3	0.92
CS67-3G25	233.8	231.6	0.99
CS40-3G20/12	192.5	199.4	1.04
CS40-3G20	219.0	226.2	1.03

4.2.3. Load–deflection responses

Fig. 24 compares the load–deflection curves obtained from the FE simulations and those from the tests. As shown in Fig. 24, the load–deflection responses of either the control specimen or the FRP-CZC beams can be closely predicted using the proposed FE approach. For the control specimen CB, the load experienced a rapid drop once crushing of the top concrete cover occurred, as shown in Fig. 24(a). For the FRP-CZC beams, the predicted load–deflection curves exhibit an ascending second branch or plateau depending on the compressive behavior of the FRP-confined concrete core, as shown in Figs. 24(b)–(f).

Although the FE predictions generally agree with the test results, certain limitations of the modeling approach should be acknowledged. The proposed FE approach was validated only for beams with circular FRP spiral confinement and normal-strength concrete; its applicability to rectangular spirals, discrete hoops, or higher-strength concretes requires further verification. In addition, a perfect bond between FRP bars and concrete was assumed, and potential bond–slip effects were not explicitly considered. These assumptions may influence local stress distributions and failure characteristics.

5. Conclusions

This paper has presented a combined experimental and numerical study on an innovative sectional form for FRP bar-reinforced

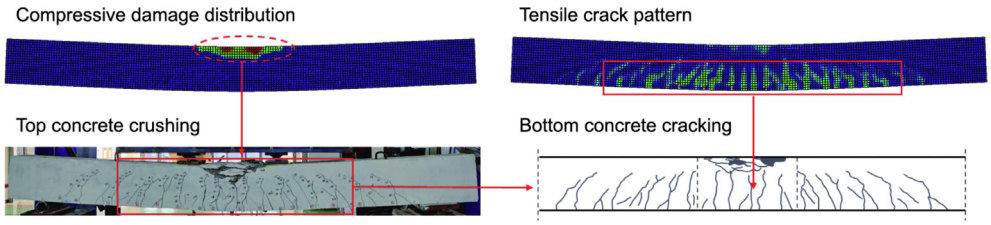

Fig. 21. Comparison of TC failure between FE simulation and test (Specimen CB).

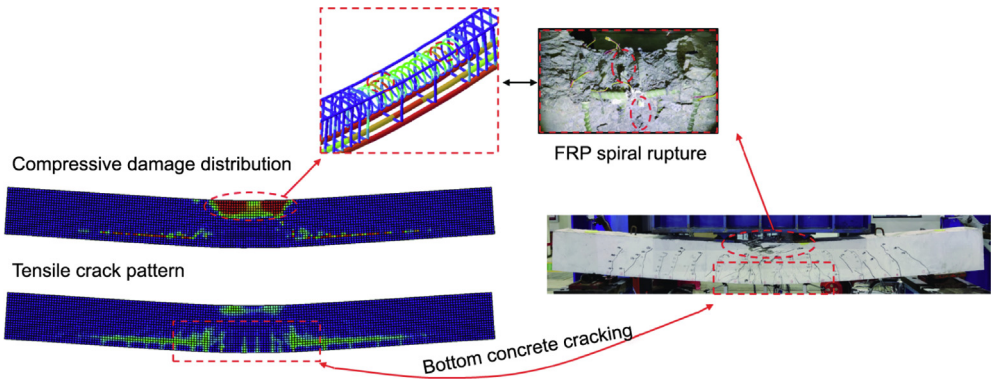

Fig. 22. Comparison of RFS + CC failure between FE simulation and test (Specimen CS40-3G25).

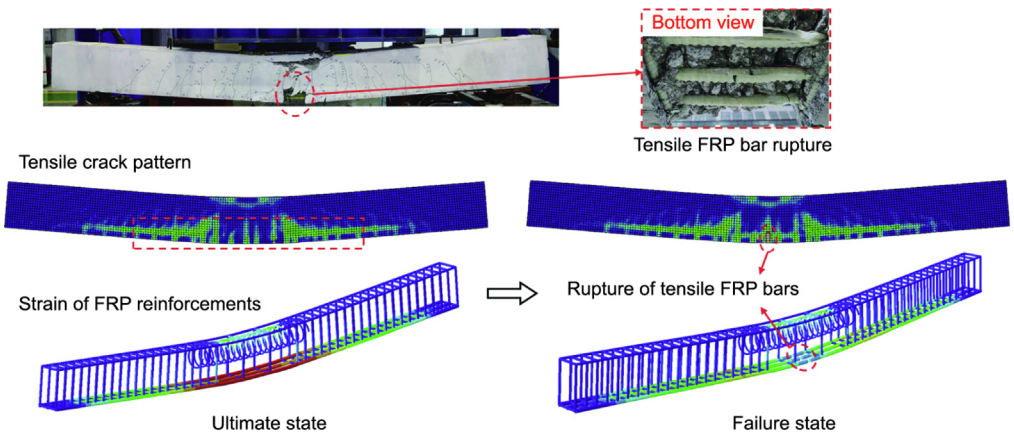

Fig. 23. Comparison of RT failure between FE simulation and test (Specimen CS40-3G20).

Please cite this article as: S.-S. Zhang, X.-B. Hu and J.-G. Teng, Imparting Ductility to FRP-Reinforced Concrete Beams Through Compression Zone Confinement, Engineering, https://doi.org/10.1016/j.eng.2026.04.012

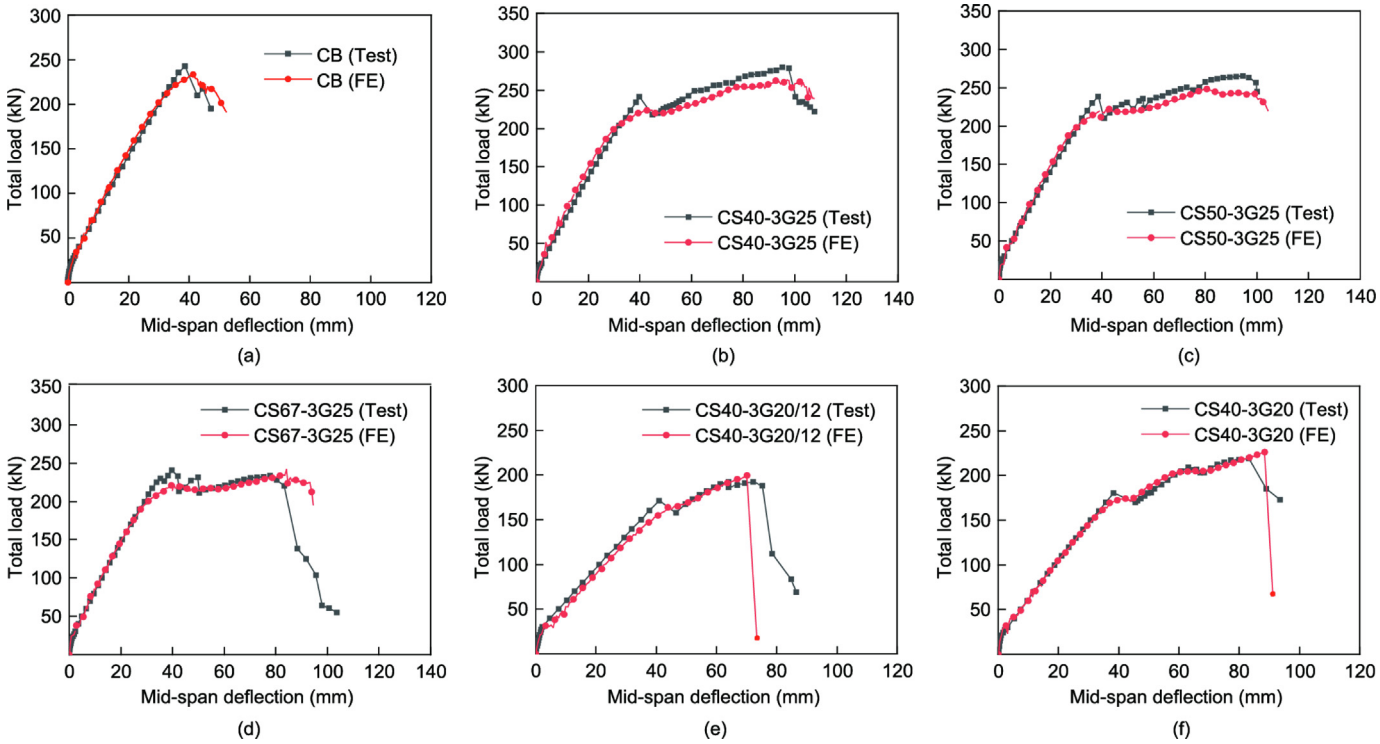

Fig. 24. Comparison of load–deflection curves between FE simulations and tests. (a) CB; (b) CS40-3G25; (c) CS50-3G25; (d) CS67-3G25; (e) CS40-3G20/12; (f) CS40-3G20.

concrete (FRP-RC) beams with compression-zone confinement (CZC) from FRP spirals/hoops to achieve ductile flexural behavior. Eight large-scale simply supported FRP–RC beams, including one control beam and seven FRP-CZC beams, were tested in four-point bending. The parameters examined in this study included the pitch of the FRP spiral, longitudinal tension FRP reinforcement ratio, and FRP confinement configuration. A 3D nonlinear FE approach was established, in which a dynamic analysis approach was employed to trace the load–deflection path. The following conclusions can be drawn from the analyses and discussion of the FE predictions and test results:

(1) The confinement of concrete in the compression zone with FRP spirals/hoops can greatly enhance the ductility of FRP-RC beams and simultaneously lead to a significant increase in their ultimate loads. The FRP confinement effect is progressively activated after the spalling of top concrete cover, resulting in a ductile "yield plateau" in the load–deflection curve of FRP-CZC beams. In this study, the ductility index μ_e and the ultimate load of the best-performing FRP-CZC beam (Specimen CS40-3G25) are 150.0% and 12.8% greater, respectively, than those of the control beam that had no FRP confinement. Notably, comparing Specimens CS40-3G25 with CB reveals that the energy-based ductility index increased by 150% with only about a 7% increase in FRP material cost, indicating a highly favorable cost–performance ratio for practical applications.

(2) The circular FRP spiral confinement was found to be significantly more effective than the rectangular FRP spiral confinement in enhancing the flexural performance of FRP-RC beams. This is easy to understand because a circular FRP spiral provides stronger confinement to the concrete in the compression zone than a rectangular FRP spiral. A continuous circular FRP spiral also showed better confinement performance than discrete circular FRP hoops because slippage between the two ends in the overlapping zone of an FRP hoop could occur during the loading process. However, by better anchoring the two ends of an FRP hoop into the concrete (e.g., with a longer overlapping zone), the confinement effect from circular FRP hoops can be similar to that of a continuous circular spiral.

(3) An FRP spiral with a smaller pitch (i.e., a higher volumetric ratio) led to a stronger confinement effect, resulting in a higher level of ductility and a higher ultimate load for the beam. The level of FRP confinement can be designed to achieve a desired flexural behavior for FRP-CZC beams. In the present study, the ductility index μ_{d1} and the ultimate load of the FRP-CZC beam with a spiral pitch of 40 mm are 18.3% and 19.8% greater, respectively, than those of the FRP-CZC beam with a spiral pitch of 67 mm.

(4) The longitudinal tension FRP reinforcement ratio should be properly designed such that the confinement effect from the FRP spiral/hoops to the concrete in the compression zone can be utilized more fully. In the present study, beams with a relatively low longitudinal tension FRP reinforcement ratio failed owing to the rupture of tension FRP bars, resulting in an incomplete activation of FRP confinement, whereas beams with a higher longitudinal FRP reinforcement ratio exhibited a much more ductile failure process as a result of a fuller activation of FRP confinement.

(5) The proposed FE approach provided accurate predictions of the ultimate load, failure mode, and load–deflection response of FRP-CZC beams with circular FRP spiral confinement in the compression zone. The proposed FE approach can be adopted in future parametric studies to further examine the effects of various parameters on the behavior of FRP-CZC beams, thereby serving as a valuable tool for developing a better understanding of these novel beams and establishing a robust design theory for them.

The present study demonstrated the effectiveness of improving the ductility of FRP-RC beams through the provision of FRP spiral confinement to the compression zone concrete. Such FRP-CZC beams thus have great potential for practical applications in corrosive environments (e.g., marine environments) because they possess both the durability and ductility features normally required for such applications. Since the current findings are based on monotonic four-point bending tests of simply supported beams with normal-strength concrete, further investigations into their

Please cite this article as: S.-S. Zhang, X.-B. Hu and J.-G. Teng, Imparting Ductility to FRP-Reinforced Concrete Beams Through Compression Zone Confinement, Engineering, https://doi.org/10.1016/j.eng.2026.04.012

performance under other loading and support conditions as well as other concrete strength grades remain to be undertaken. Such studies would help the development of an in-depth understanding of the behavior of FRP-CZC beams and support its broader implementation in design practice.

CRediT authorship contribution statement

Shi-Shun Zhang: Writing – review & editing, Validation, Supervision, Resources, Methodology. **Xiao-Bing Hu:** Writing – original draft, Methodology, Investigation. **Jin-Guang Teng:** Writing – review & editing, Supervision, Methodology, Conceptualization.

Declaration of competing interest

The authors declare that they have no known competing financial interests or personal relationships that could have appeared to influence the work reported in this paper.

Acknowledgments

The authors are grateful for the financial support received from the National Natural Science Foundation of China (52078231), the Key Research and Development Program of Hubei Province of China (2021BCA150), and the Hong Kong Research Grants Council (T22-502/18-R). During the writing process of this article, AI technology was used to enhance the language quality.

References

[1] Pilakoutas K, Neocleous K, Guadagnini M. Design philosophy issues of fiber reinforced polymer reinforced concrete structures. J Compos Constr 2002;6(3):154–61.
[2] Karbhari VM, Chin JW, Hunston D, Benmokrane B, Juska T, Morgan R, et al. Durability gap analysis for fiber-reinforced polymer composites in civil infrastructure. J Compos Constr 2003;7(3):238–47.
[3] Hollaway LC, Teng JG. Strengthening and rehabilitation of civil infrastructures using fibre-reinforced polymer (FRP) composites. Cambridge: Woodhead Publishing; 2008.
[4] Liu KC, Jiang C, Yu T, Teng JG. Compressive behaviour of elliptical FRP tube-confined concrete columns. Compos Struct 2023;303:116301.
[5] Ueda T. Material mechanical properties necessary for the structural intervention of concrete structures. Engineering 2019;5(6):1131–8.
[6] Smits J. Fiber-reinforced polymer bridge design in the Netherlands: architectural challenges toward innovative, sustainable, and durable bridges. Engineering 2016;2(4):518–27.
[7] Ceroni F, Cosenza E, Gaetano M, Pecce M. Durability issues of FRP rebars in reinforced concrete members. Cem Concr Compos 2006;28(10):857–68.
[8] Kassem C, Farghaly AS, Benmokrane B. Evaluation of flexural behavior and serviceability performance of concrete beams reinforced with FRP Bars. J Compos Constr 2011;15(5):682–95.
[9] Elgabbas F, Vincent P, Ahmed EA, Benmokrane B. Experimental testing of basalt–fiber-reinforced polymer bars in concrete beams. Compos Pt B Eng 2016;91:205–18.
[10] Barris C, Torres L, Turon A, Baena M, Catalan A. An experimental study of the flexural behaviour of GFRP RC beams and comparison with prediction models. Compos Struct 2009;91(3):286–95.
[11] Zou PXW. Flexural behavior and deformability of fiber reinforced polymer prestressed concrete beams. J Compos Constr 2003;7(4):275–84.
[12] Zhou YW, Wu YF, Teng JG, Leung AYT. Ductility analysis of compression-yielding FRP-reinforced composite beams. Cem Concr Compos 2009;31(9):682–91.
[13] Nanni A. Flexural behavior and design of RC members using FRP reinforcement. J Struct Eng 1993;119(11):3344–59.
[14] El-Nemr A, Ahmed EA, Benmokrane B. Flexural behavior and serviceability of normal- and high-strength concrete beams reinforced with glass fiber-reinforced polymer bars. ACI Struct J 2013;110(06):1077–87.
[15] Maranan GB, Manalo AC, Benmokrane B, Karunasena W, Mendis P. Evaluation of the flexural strength and serviceability of geopolymer concrete beams reinforced with glass–fibre-reinforced polymer (GFRP) bars. Eng Struct 2015;101:529–41.
[16] Lau D, Pam HJ. Experimental study of hybrid FRP reinforced concrete beams. Eng Struct 2010;32(12):3857–65.
[17] Wu YF. Ductility demand of compression yielding fiber-reinforced polymer-reinforced concrete beams. ACI Struct J 2008;105(1):104–10.
[18] Wu YF. New avenue of achieving ductility for reinforced concrete members. J Struct Eng 2006;132(9):1502–6.
[19] Wu YF, Jiang JF, Liu K. Perforated SIFCON blocks—an extraordinarily ductile material ideal for use in compression yielding structural systems. Constr Build Mater 2010;24(12):2454–65.
[20] Teng JG, Zhang B, Zhang SS, Fu B. Steel-free hybrid reinforcing bars for concrete structures. Adv Struct Eng 2018;21(16):2617–22.
[21] Zhang SS, Liu YX, Ke Y, Nie XF, Yu T. Novel FRP-RC beams with ductile FRP-UHPC hybrid rebars in the compression zone: flexural behaviour. Constr Build Mater 2025;460:139758.
[22] Wang HZ, Belarbi A. Ductility characteristics of fiber-reinforced-concrete beams reinforced with FRP rebars. Constr Build Mater 2011;25(5):2391–401.
[23] Yuan F, Pan JL, Leung CKY. Flexural behaviors of ECC and concrete/ECC composite beams reinforced with basalt fiber-reinforced polymer. J Compos Constr 2013;17(5):591–602.
[24] Wang HW, Xu JJ, Jiang X, Han XY, Pan KM, Yu RC, et al. Flexural behavior of GFRP-RC beams confined with CFRP in compression zone. Eng Struct 2024;302:117348.
[25] Deng X, Tang S, Tang J, Liu S, Yang S. Experimental study of the flexural performance of GFRP-reinforced seawater sea sand concrete beams with built-in GFRP tubes. Materials 2024;17(13):3221.
[26] Tahrirchi EJ, Alaee F, Jalali M. Experimental investigation of ductility in GFRP RC beams by confining the compression zone. Adv Civ Eng 2024;2024:1–21.
[27] Burgoyne CJ. Rational use of advanced composites in concrete. Proc Inst Civ Eng Struct Build 2001;146(3):253–62.
[28] Burgoyne CJ, Leung HY. Test on prestressed concrete beam with AFRP spiral confinement and external aramid tendons. In: Proceedings of the Antoine E. Naaman Symposium-Four Decades of Progress in Prestressed Concrete, FRC, and Thin Laminate Composite; 2010 Nov 11–14; Ann Arbor, MI, USA. Farmington Hills: American Concrete Institute (ACI); 2010. p. SP-272.
[29] Pantelides CP, Gibbons ME, Reaveley LD. Axial load behavior of concrete columns confined with GFRP spirals. J Compos Constr 2013;17(3):305–13.
[30] Afifi MZ, Mohamed HM, Benmokrane B. Axial capacity of circular concrete columns reinforced with GFRP bars and spirals. J Compos Constr 2014;18(1):04013017.
[31] Hu XB, Nie XF, Wang JJ, Zhang SS. Behavior of FRP spiral-confined concrete under concentric compression. Eng Struct 2024;321:118898.
[32] Hu XB, Nie XF, Wang JJ, Yu T, Zhang SS. Experimental study on GFRP spiral-confined concrete under eccentric compression. Compos Struct 2025;354:118793.
[33] Ministry of Housing and Urban-Rural Development of the People's Republic of China. GB 50608–2020: Technical standard for fiber reinforced polymer (FRP) in construction. Chinese standard. Beijing: China Architecture and Building Press; 2020. [Chinese].
[34] American Society for Testing and Materials (ASTM). ASTM C39/C39M-18: Standard test method for compressive strength of cylindrical concrete specimens. ASTM standard. West Conshohocken: ASTM; 2018.
[35] American Society for Testing and Materials (ASTM). ASTM D7205/D7205M-11: Standard test method for tensile properties of fiber reinforced polymer matrix composite bars. West Conshohocken: ASTM; 2011.
[36] International Organization for Standardization (ISO). ISO 104061-1:2015: Fibre-reinforced polymer (FRP) reinforcement of concrete: test methods: part 1: FRP bars and grids. Geneva: ISO; 2015.
[37] Huang ZJ, Chen WS, Tran TT, Pham TM, Hao H, Chen ZY, et al. Experimental and numerical study on concrete beams reinforced with basalt FRP bars under static and impact loads. Compos Struct 2021;263:113648.
[38] Al-Sunna R, Pilakoutas K, Hajirasouliha I, Guadagnini M. Deflection behaviour of FRP reinforced concrete beams and slabs: an experimental investigation. Compos Pt B Eng 2012;43(5):2125–34.
[39] Adam MA, Said M, Mahmoud AA, Shanour AS. Analytical and experimental flexural behavior of concrete beams reinforced with glass fiber reinforced polymers bars. Constr Build Mater 2015;84:354–66.
[40] Elgabbas F, Ahmed EA, Benmokrane B. Flexural behavior of concrete beams reinforced with ribbed basalt-FRP bars under static loads. J Compos Constr 2017;21(3):04016098.
[41] Ashour SA. Effect of compressive strength and tensile reinforcement ratio on flexural behavior of high-strength concrete beams. Eng Struct 2000;22(5):413–23.
[42] Mahin SA, Bertero VV. Problems in establishing and predicting ductility in structural design. In: Proceedings of the International Symposium on Earthquake Structural Engineering; 1976 Aug 19–21; St. Louis, MO, USA. Washington, DC: National Science Foundation; 1976. p. 613–28.
[43] Park R. Evaluation of ductility of structures and structural assemblages from laboratory testing. Bull N Z Soc Earthq Eng 1989;22(3):155–66.
[44] Naaman AE, Jeong SM. Structural ductility of concrete beams prestressed with FRP tendons. In: Proceedings of the 2nd International RILEM Symposium on Non-metallic (FRP) Reinforcement for Concrete Structures; 1995 Aug 23–25; Ghent, Belgium. Boca Raton: CRC Press; 1995. p. 379–86.
[45] ABAQUS. ABAQUS analysis user's manual (version 6.14). Mayfield Heights: Dassault Systèmes SIMULIA Corporation; 2014.
[46] Zeng JJ, Ye YY, Liu WT, Zhuge Y, Liu Y, Yue QR. Behaviour of FRP spiral-confined concrete and contribution of FRP longitudinal bars in FRP-RC columns under axial compression. Eng Struct 2023;281:115747.

Please cite this article as: S.-S. Zhang, X.-B. Hu and J.-G. Teng, Imparting Ductility to FRP-Reinforced Concrete Beams Through Compression Zone Confinement, Engineering, https://doi.org/10.1016/j.eng.2026.04.012

[47] Ministry of Housing and Urban-Rural Development of the People's Republic of China. GB 50010–2010: Code for design of concrete structures. Chinese standard. Beijing: China Architecture & Building Press; 2010. Chinese.
[48] American Concrete Institute (ACI). ACI-318: Building code requirements for structural concrete and commentary. ACI standard. Farmington Hills: ACI; 2019.
[49] Zinkaah OH, Alridha Z, Alhawat M. Numerical and theoretical analysis of FRP reinforced geopolymer concrete beams. Case Stud Constr Mater 2022;16:e01052.
[50] Nie XF, Zhang SS, Chen GM, Yu T. Strengthening of RC beams with rectangular web openings using externally bonded FRP: numerical simulation. Compos Struct 2020;248:112552.
[51] Ke Y, Zhang SS, Nie XF, Yu T, Yang YM, Jedrzejko MJ. Finite element modelling of RC beams strengthened in flexure with NSM FRP and anchored with FRP U-jackets. Compos Struct 2022;282:115104.
[52] Zhang SS, Zhang DD, Nie XF. Behavior of RC interior beam-to-column joints with FRP-strengthened beam web openings under cyclic loading. Eng Struct 2025;324:119373.

Please cite this article as: S.-S. Zhang, X.-B. Hu and J.-G. Teng, Imparting Ductility to FRP-Reinforced Concrete Beams Through Compression Zone Confinement, Engineering, https://doi.org/10.1016/j.eng.2026.04.012